KSOE

Journal of Ocean Engineering and Technology 38(5), 199–209, October, 2024
https://doi.org/10.26748/KSOE.2024.071

pISSN 1225-0767
eISSN 2287-6715

Original Research Article

Analysis of the Impact of Dynamic Operation of PEMFCs for Ship Applications

Jae Hong Kim[1], Seon Hyeong Lee[1], Jae Heon Kwon[1], Ryu Bin Kwon[1], Kwang Hyo Jung[2], Moonho Son[3] and Hyun Park[2]

[1]*Graduate Student, Department of Naval Architecture and Ocean Engineering, Pusan National University, Busan, Republic of Korea*
[2]*Professor, Department of Naval Architecture and Ocean Engineering, Pusan National University, Busan ,Republic of Korea*
[3]*Senior Researcher, Carbon Reduction Department, Samsung Heavy Industries R&D Center, Seongnam, Republic of Korea*

KEYWORDS: Polymer electrolyte membrane fuel cell, Single cell, Ship operation profile, Dynamic load, Static load, Degradation rate

ABSTRACT: *Dynamic responses of polymer electrolyte membrane fuel cells (PEMFC) were analyzed under varying loads to understand the performance of PEMFCs for ship applications. Experiments employing single cells were conducted under a static load with a constant current of 6.64 A and dynamic loads at a ramp rate of 2.5%/s and 5.0%/s, representing a simplified ship operation condition. Under the static load, the voltage drop was 0.054 V at 1.00 A/cm^2 and was dominant below 0.40 A/cm^2. In contrast, under the dynamic load (5.0%/s ramp rate), the voltage drop was 0.061 V at 1.00 A/cm^2 and was dominant above 0.40 A/cm^2, with similar behavior observed at the ramp rate of 2.5%/s. To compare performance across load conditions, degradation rates were calculated through linear regression of the voltage drop for each current density. The degradation rate at 1.00 A/cm^2 was 0.143 mV/h under static load conditions and 0.174 mV/h under dynamic load conditions (ramp rate: 5.0%/s), indicating approximately 21% greater degradation rates than those observed under static load conditions. These experimental results provide foundational data for PEMFC performance analysis, particularly regarding performance degradation caused by dynamic loads in marine environments.*

1. Introduction

Emissions from conventional ship engines powered by fossil fuel combustion have been identified as a significant contributor to climate change. In response, the transition from fossil fuels to alternative energy sources has been accelerated worldwide, particularly following Marine environment protection committee (MEPC) 80 of the International maritime organization (IMO), which set the goal of achieving net-zero carbon emissions for ships. Lee et al. (2022) suggested the applicability of polymer electrolyte membrane fuel cells (PEMFCs), which utilize hydrogen fuel, through a life cycle assessment of marine gas oil, liquefied natural gas, and hydrogen, all of which are considered eco-friendly alternative fuels. PEMFCs generate electrical energy by utilizing the flow of electrons along external circuits during the reaction of hydrogen and oxygen to produce water. Due to their high power density, low operating temperature, and rapid start-up/shut-down capabilities, PEMFCs have become the focus of research aimed at developing them as the primary power source for next-generation ships (Elkafas et al., 2022). The performance of PEMFCs is affected by the load, temperature, humidity, and flow rate (Hassani et al., 2020; Hou et al., 2012; Wasterlain et al., 2010). As PEMFC performance can be affected by load fluctuations during operation, research into their dynamic characteristics under real-world ship operating conditions is necessary.

Previous attempts to investigate the dynamic characteristics of PEMFCs have utilized load profiles. For vehicles, Meng et al. (2021) conducted research on the effects of dynamically changing hydrogen and oxygen flow rates on PEMFC performance degradation for simplified load profiles, identifying starvation during changes in gas flow rates as the primary cause of degradation. Chu et al. (2022) analyzed the performance degradation mechanism over a 2,500-hour driving experiment under a fuel cell dynamic load cycle (FC-DLC), simulating the operating load of a vehicle, and found that the reversible oxidation of platinum was the main cause of performance degradation. Zuo et al. (2021) contributed to the prediction of PEMFC lifespan by analyzing electrochemical impedance spectroscopy, cyclic

Received 29 August 2024, revised 5 October 2024, accepted 6 October 2024
Corresponding author Hyun Park: +82-51-510-2730, hyunpark@pusan.ac.kr

voltammetry, and linear sweep voltammetry data from a 1,000-hour FC-DLC experiment.

In the maritime sector, Gadducci et al. (2022) developed a protocol incorporating the load profile of a tourist boat, provided by Fincantieri, to evaluate the dynamic load response of a ship's power generation system equipped with PEMFCs. Their balance of plant (BoP) analysis underscored the importance of heat and humidity management in enhancing the performance and longevity of fuel cell systems on ships. Saponaro et al. (2024) analyzed the impact of heat management on performance degradation in electric propulsion ferries equipped with PEMFC systems. They developed a hybrid model combining PEMFCs and an energy storage system to simulate power output under dynamic loads. However, most studies on PEMFCs in maritime applications have focused primarily on system output, with limited research dedicated to analyzing performance degradation under dynamic ship loads.

In the field of material engineering, Research to quantify PEMFC performance degradation typically involves calculating degradation rates, which represent the voltage reduction rate over time. Cleghorn et al. (2006) performed a 26,300-hour continuous operation experiment with 800 mA/cm^2. They highlighted the decomposition of electrolyte membranes as the dominant cause of performance degradation at the current density through the degradation rate comparison. Cheng et al. (2003) performed a 1,000-hour experiment with a PEMFC utilizing ruthenium oxide (RuO_2) as the anode catalyst, reporting additional degradation after 700 h due to catalyst particle coalescence. Chung et al. (2009) compared degradation rates over various operational periods—early (40 h), middle (40 to 300 h), and long-term (after 300 h)—identifying platinum particle agglomeration, dissolution, and membrane electrode assembly (MEA) property improvements as the dominant factors influencing performance at each stage.

This study aims to investigate the performance characteristics of PEMFCs under changing ship load conditions as part of ongoing research on their potential as power sources for ships. The experimental results presented herein provide valuable baseline data for analyzing PEMFC performance degradation caused by dynamic ship loads.

2. Experimental Details

2.1 PEMFC Single Cell and Test Station

In this study, a single cell was used in the experiment instead of a stack for which the effects of internal factors (e.g., heat management and water discharge) cannot be ignored (Park and Choe, 2008). For the single cell used, the MEA, gas diffusion layer (GDL), gasket, and unit cell parts were assembled using the same torque (9.04 N·m) at ambient temperature under atmospheric conditions. The MEA (15 μm, Gore, America) used a model with a size of 5.0 × 5.0 cm^2, and it was prepared by loading Pt with a content of 0.4 mg/cm^2 on carbon catalysts at both the anode and cathode. GDL (Sigracet 39BB, SGL, Germany) and the gasket (215 μm, SGL, Germany) were used to efficiently supply the H_2 and air required for reactions. The unit cell components (CNL Energy, South Korea) consist of bipolar plates (BPs), current collectors (CCs), and end plates (EPs), which constitute the exterior of the single cell. Graphite, Ag-plated Cu, and anodized Al were used for the BPs, CCs, and EPs, respectively.

The test station setup consisted of two test benches, designed to evaluate two single cells simultaneously. Each single-cell station was equipped with a mass flow controller (MFC) and an electronic load to regulate and measure parameters such as flow rate, temperature, humidity, and load, as depicted in Fig. 1. A bubbler-type humidifier (Pureun Tech Energy, South Korea) was used to humidify the gas entering the anode and cathode. The gas was introduced into the humidifier, where it passed through liquid in the form of bubbles before being humidified. The humidified gas was then heated via a line heater capable of reaching 200 °C, ensuring that the desired inlet temperature was maintained before entering the single cell. The flow rates of N_2, H_2, and air entering each single-cell test station were

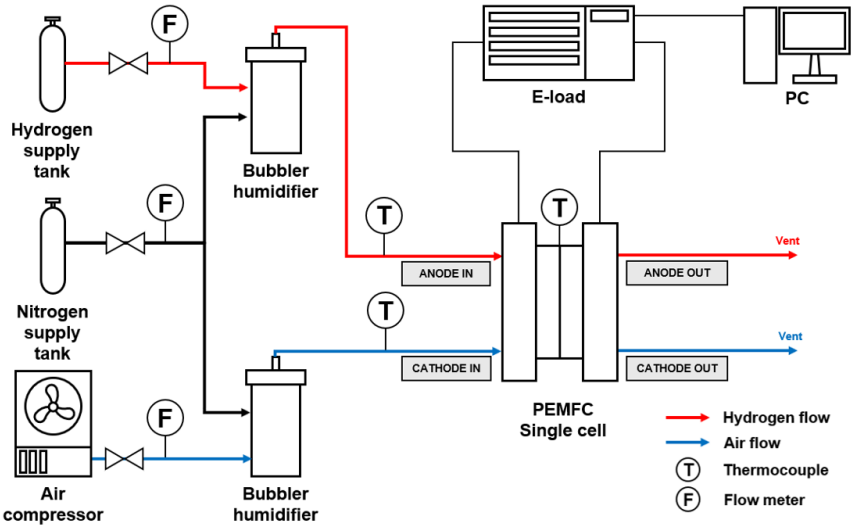

Fig. 1 Schematic view of single cell test station

controlled using the MFC (EL-FLOW classic F-201CL, Bronkhorst, Netherlands). Temperature regulation and monitoring of the single cell were achieved using a heated rod and a thermocouple (Sunglim Inc., South Korea). The thermocouple used was of the K type, capable of measuring temperatures ranging from −200 °C to 1,250 °C.

2.2 Electronic Load and Measurement

In this study, an electronic load (PLZ-405W, Kikusui, Japan) with a range of 0 to 80 A and 0 to 15.75 V was used to apply a load to the single cell. The voltage and current measurements for the IV curve were also conducted using this electronic load. The measurements followed the protocol recommended by the cell manufacturer (CNL Energy), as illustrated in Fig. 2. Currents corresponding to an open circuit voltage (OCV) down to 0.40 V were recorded. The voltage measurements were taken three times, and the average value was used for analysis. A lower voltage limit of 0.40 V was established to prevent damage to the single cell caused by excessive current generation when the output voltage was low. The time allocated for measuring the output voltage was 30 s at OCV, while one minute was allotted for each current density, ensuring the voltage deviation remained below 5 mV, as specified in International Electrotechnical Commission (IEC) 62282-7-1 standards (International Electrotechnical Commission, 2017). The sampling rate was set at 1 Hz, and for accuracy, only the data from the final 10 s of the one-minute measurement period were used, ensuring sufficient stabilization of results. In terms of flow rate, a stoichiometric ratio of 1.5 for hydrogen and 2.0 for air was applied. When the current exceeded 10.0 A, the flow rate corresponding to each current value was employed. For currents below 10.0 A, the flow rate corresponding to 10.0 A was used to maintain the appropriate temperature and humidity of the inlet gas. The flow rate for each current value was calculated using Eq. (1) (as derived from Faraday's law (O'hayre et al., 2016)).

$$Q_{I,\lambda} = \frac{M \times I \times \lambda \times n}{z \times F \times \rho \times \phi} \quad (1)$$

In Eq. (1), Q is the volumetric flow rate (L/s), M is the molar mass (g/mol), I is the current applied to the cell (A), λ is the stoichiometric ratio of each flow rate, n is the number of cells, z is the charge number, F is the Faraday constant (C/mol), ρ is the density of the inlet gas (g/dm^3), and ϕ is the mole fraction of the gas.

The flow rates of the gas introduced into the anode and cathode, calculated using Eq. (1), are expressed as Eqs. (2) and (3), respectively.

$$Q_{Hydrogen} = 6.97 \times I \times \lambda_a \times n \quad (2)$$

$$Q_{Air} = 16.7 \times I \times \lambda_c \times n \quad (3)$$

In the above Eqs. (2) and (3), λ_a and λ_c represent the stoichiometric ratios of the anode and cathode, respectively.

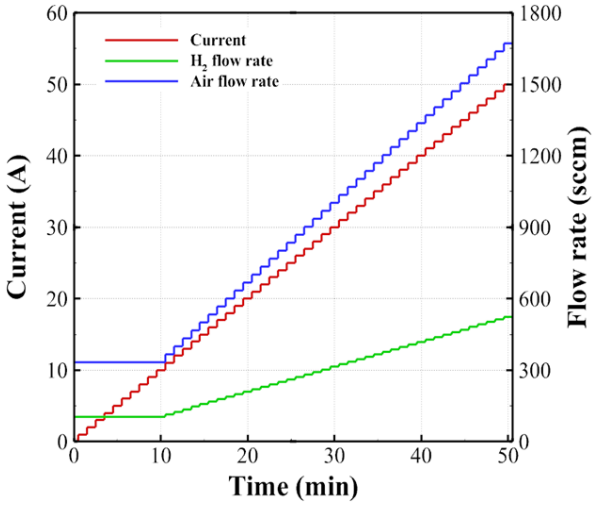

Fig. 2 IV curve measurement protocol follows these guidelines: For current values exceeding 10.0 A, the flow rate corresponding to each specific current is applied. For current values below 10.0 A, the flow rate equivalent to that at 10.0 A is used to regulate the temperature and humidity of the inlet gas.

2.3 Conditions of Case Study

In this study, 99.99% pure hydrogen and compressed air were humidified using a bubbler-type humidifier. The flow rate of these gases was controlled via the MFC before being introduced into the single cell. The operating temperature of the single cell during the experiment was maintained at 70 °C. To ensure that the relative humidity of the inlet gas inside the single cell remained at 100%, the internal temperature of the bubbler-type humidifier was also set to 70 °C, matching the temperature inside the single cell.

The single cells used in the experiment were activated following the prescribed activation protocol, as shown in Fig. 3. This protocol, based on the IEC 62282-7-1 guidelines, was recommended by the cell manufacturer (CNL Energy, South Korea). The activation process involved the following steps: (1) maintaining the load for 5 s at open circuit voltage (OCV), (2) decreasing the load voltage by 0.05 V, from 0.90 to 0.40 V, at ten-second intervals, (3) maintaining the voltage at 0.40 V for one minute, and (4) increasing the voltage by 0.05 V, from 0.40 to 0.90 V, every 10 s. The activation was repeated until the voltage deviation remained below 5 mV for five continuous hours, in accordance with the voltage stabilization criteria outlined in IEC 62282-7-1. Preliminary experiments demonstrated that voltage stabilization was achieved after repeating the activation protocol 60 times in constant voltage (CV) mode. Therefore, in this study, it was determined that voltage stabilization was reached after 60 repetitions of the protocol. During the activation process, the flow rates of hydrogen and air were fixed at 700 mL/min and 3,000 mL/min, respectively, based on the manufacturer's recommendations. Pre-tests confirmed that no flooding occurred at these flow rates.

Experiments under both static and dynamic load conditions were conducted for three fully activated single cells. In the static load condition experiment, the performance degradation of the single cells

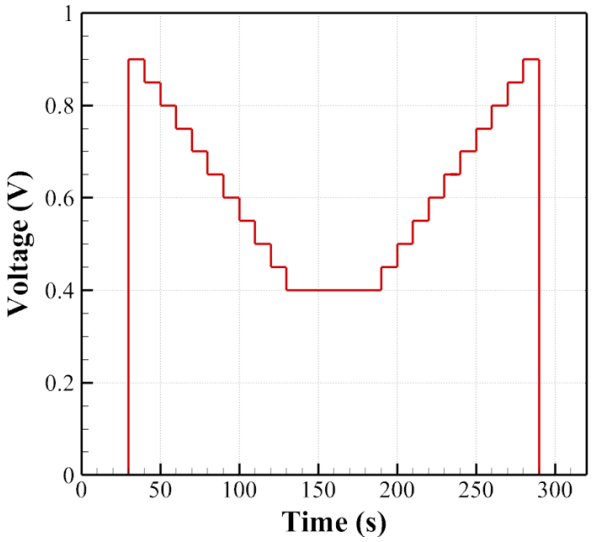

Fig. 3 Activation protocol carried in accordance with the MEA and component manufacturer's instructions (repeated 60 cycles for stabilizing voltage)

was evaluated by maintaining a constant current (CC). The load current was set at 6.64 A, corresponding to a voltage of 0.75 V, which is commonly used in stationary fuel cells. This current value was selected based on previous research in the field of PEMFCs (Lee et al., 2010; Oh et al., 2018). The current was derived from the initial IV curve measurements taken after the installation of the single cell. In this study, the IV curve was measured every 24 h during the first nine measurement intervals to capture the trend of the initial phase, where the IV curve undergoes rapid changes. In the relatively stable mid-to-late phase, the IV curve was measured every 72 h to minimize the potential influence of the measurement process on the overall results.

In the dynamic load condition experiment, the load was increased at rates of 2.5%/s and 5.0%/s in two single cells, respectively, to examine the effect of different ramp rates on performance. The load profile (Fig. 4) was derived by simplifying ship operation data and comprised four phases: loading, unloading, maneuvering, and seagoing. A full load cycle required 1,520 s to complete, and the cycle was repeated 900 times to experimentally assess the performance degradation caused by dynamic loads. For the seagoing phase, the load was set to match the output corresponding to 0.60 V from the initial IV curve, while the load for the normal continuous rating (NCR) operation was set at 100%. The loads for the loading, unloading, and maneuvering phases were set to 17%, 32%, and 66% of the seagoing load, respectively. To facilitate a direct comparison with the static load condition, the electronic load was operated in CC mode. The corresponding current for each load phase was calculated and applied during the experiment. For a ramp rate of 2.5%/s, the current values were 2.28 A for loading, 4.53 A for unloading, 10.36 A for maneuvering, and 17.80 A for seagoing. For a ramp rate of 5.0%/s, the values were 2.60 A for loading, 5.13 A for unloading, 11.70 A for maneuvering, and 20.53 A for seagoing. The voltage and current conditions used were simplified based on actual LNG carrier operational data. To simulate a scenario where ships are operating at 80% of NCR, a voltage of 0.60 V, representing 80% of the standard 0.75 V used in fuel cells, was applied.

To monitor performance changes, the IV curve was measured every 50 cycles for the first 150 cycles to capture the trends during the initial phase, where rapid changes in the IV curve occur. During the relatively stable mid-to-late phase, the IV curve was measured every 150 cycles to minimize the impact of measurement on the experimental results. For consistency, the conditions for IV curve measurements under dynamic

Table 1 Summary of experimental conditions

Experimental condition	Voltage (V)	Current (A)
CC mode	0.75	6.64
Dynamic load condition (2.5%/s of ramp rate)	0.80	2.28
	0.76	4.53
	0.68	10.36
	0.60	17.80
Dynamic load condition (5.0%/s of ramp rate)	0.81	2.60
	0.77	5.13
	0.70	11.70
	0.60	20.53

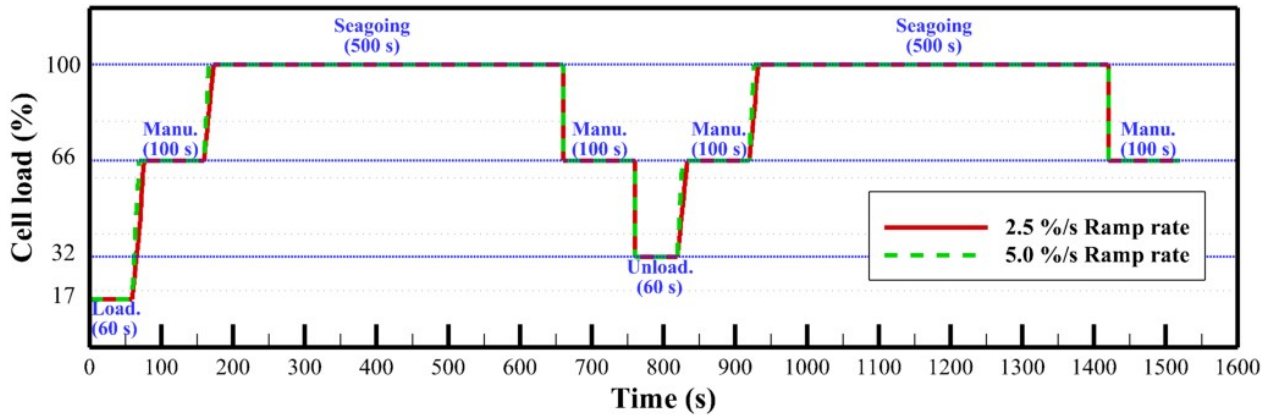

Fig. 4 Simplified ship operation profile where ramp rate is 2.5%/s, 5.0%/s

Table 2 Details of experimental conditions when the ramp rate is 2.5%/s

Step	Percent of power (%)	Total duration (s)	Current (A)	Cell voltage (V)	Percent of time (%)
Loading	17	60	2.28	0.80	3.95
Unloading	32	60	4.53	0.76	3.95
Maneuvering	66	400	10.36	0.68	26.3
Seagoing	100	1,000	17.80	0.60	65.8

Table 3 Details of experimental conditions when the ramp rate is 5.0%/s

Step	Percent of power (%)	Total duration (s)	Current (A)	Cell voltage (V)	Percent of time (%)
Loading	17	60	2.60	0.81	3.95
Unloading	32	60	5.13	0.77	3.95
Maneuvering	66	400	11.70	0.70	26.3
Seagoing	100	1,000	20.53	0.60	65.8

load were maintained at the same values as in the static load condition. Specifically, the humidifier temperature (70 °C), line heater temperature (80 °C), and cell operating temperature (70 °C) were kept constant. Additionally, the stoichiometric ratio of hydrogen to air was maintained at 1.5:2.0, identical to the static load condition. Tables 1 to 3 summarize the experimental conditions established through the described method.

3. Results and Discussion

3.1 Static Load (Constant Current Condition)

Table 4 presents the voltage as a function of current density over time during the static load experiment, in which a CC was applied. Figs. 5(a) and 5(b) illustrate the IV and power curves at both the initial

Table 4 Voltage drop over time at a CC of 6.64 A

Current Density (A/cm^2)	Voltage (V)								
	Initial	21 h	42 h	63 h	127 h	190 h	253 h	317 h	380 h
0.00	0.96	0.95	0.95	0.95	0.94	0.93	0.93	0.93	0.93
0.20	0.77	0.76	0.76	0.76	0.76	0.75	0.75	0.74	0.74
0.40	0.71	0.70	0.70	0.70	0.70	0.69	0.68	0.67	0.67
0.60	0.66	0.66	0.66	0.65	0.65	0.64	0.63	0.62	0.61
0.80	0.62	0.61	0.61	0.61	0.60	0.59	0.58	0.57	0.56
1.00	0.56	0.56	0.56	0.55	0.55	0.54	0.53	0.51	0.51
1.20	0.50	0.50	0.49	0.49	0.49	0.48	0.47	0.45	0.45
1.40	0.42	0.42	0.41	0.42	0.41	0.40	-	-	-

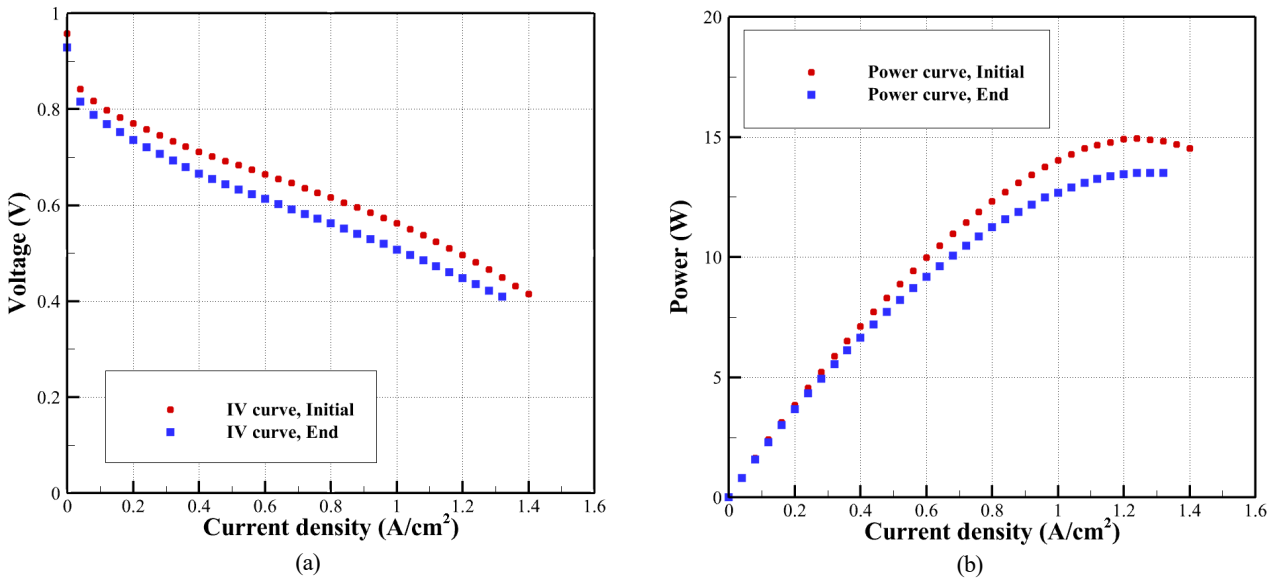

(a) (b)

Fig. 5 Comparison of (a) IV curves and (b) power curves at the initial and final stages (6.64 A CC)

and final stages of the single cell used in the static load experiment under CC conditions. The IV curve (Fig. 5a) highlights that the low current density region is predominantly affected by activation losses, which result from the reduced rate of electrochemical reactions, degradation of electrode surface performance, insufficient reactant supply, and temperature effects. The medium current density region is primarily influenced by ohmic losses due to the increased resistance of the electrolyte membranes, contact resistance between the electrodes and CCs, as well as issues with water and temperature management (Zhan et al., 2008; O'hayre et al., 2016; Tian, 2020). In Fig. 5(a), the voltage drop at a low current density (0.20 A/cm²) was measured to be 0.033 V, while at a medium current density (1.0 A/cm²), the voltage drop was 63% higher, measured at 0.054 V. Although the increased resistance of the electrolyte membranes and electrodes appeared to be the primary contributors to performance degradation under static load conditions, the two IV curves exhibited a minor difference in current density, less than 0.10 A/cm², at the final measurement point (0.40 V). The region dominated by concentration losses was not measured, but the results suggest that the degradation was mainly due to an increase in activation losses, caused by Pt particle agglomeration and dissolution, as well as an increase in ohmic losses due to electrolyte membrane wear (Paperzh et al., 2024; O'hayre et al., 2016).

In the power curve shown in Fig. 5(b), the current density that generates the maximum power output of the single cell is evident. The current density corresponding to the maximum power shifted from 1.24 to 1.28 A/cm² between the initial and final stages of the experiment. Additionally, the maximum power output decreased by approximately 10%, from 14.93 W at the initial stage to 13.51 W after PEMFC operation. These findings imply that a ship using a PEMFC as its primary power source can optimize fuel supply to meet the required load by continuously monitoring the cell's condition during operation.

3.2 Dynamic Load (Simplified Ship Operation Profile)

Table 5 presents the voltage as a function of current density over time in the dynamic load experiment, where a ramp rate of 2.5%/s was applied. Figs. 6(a) and 6(b) illustrate the IV curve and power curve, respectively, at the initial and final stages of the single cell utilized in the dynamic load experiment with a ramp rate of 2.5%/s. In Fig. 6(a), the voltage drop at a current density of 1.00 A/cm² was measured at 0.055 V, which is approximately three times greater than the voltage drop of 0.018 V observed at 0.20 A/cm². It can be inferred that the voltage drop was primarily attributed to the increase in ohmic loss rather than an increase in activation loss within this current density

Table 5 Voltage drop over time under dynamic load conditions at a ramp rate of 2.5%/s

Current density (A/cm²)	Voltage (V)								
	Initial	50 cycle	100 cycle	150 cycle	300 cycle	450 cycle	600 cycle	750 cycle	900 cycle
0.00	0.95	0.94	0.94	0.93	0.92	0.92	0.92	0.92	0.92
0.20	0.75	0.75	0.75	0.75	0.74	0.74	0.74	0.73	0.73
0.40	0.68	0.69	0.69	0.68	0.67	0.67	0.66	0.65	0.65
0.60	0.63	0.64	0.63	0.63	0.62	0.61	0.60	0.59	0.59
0.80	0.58	0.58	0.58	0.57	0.56	0.55	0.54	0.53	0.52
1.00	0.51	0.52	0.51	0.51	0.49	0.48	0.47	0.46	0.46
1.20	0.44	0.44	0.44	0.43	0.42	0.41	-	-	-

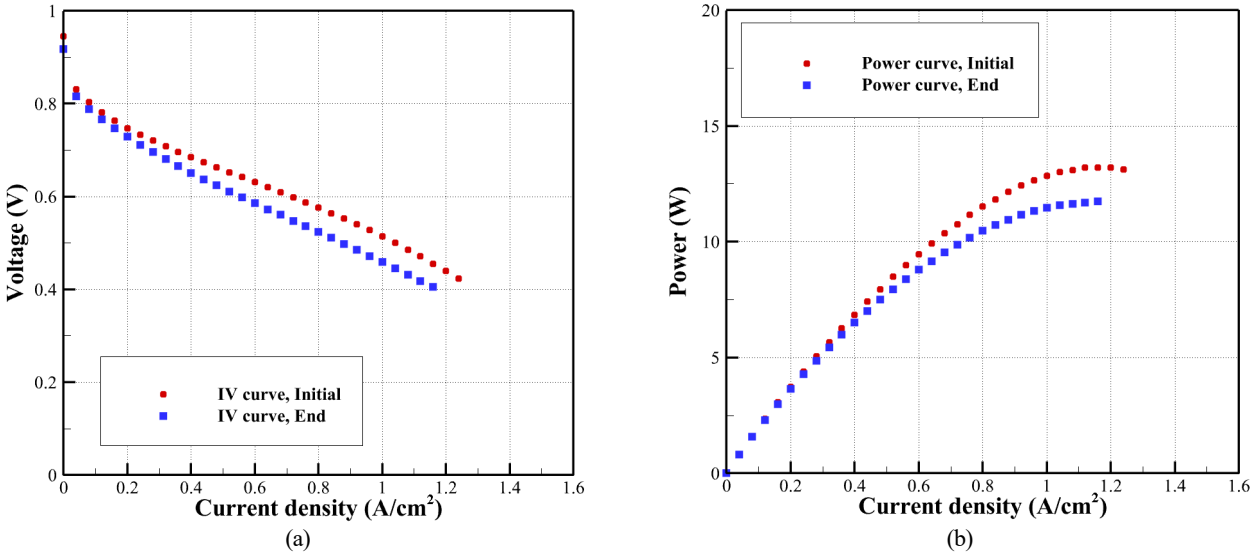

(a) (b)

Fig. 6 Comparison of (a) IV curves and (b) power curves at the initial and end stages (2.5%/s ramp rate)

Table 6 Voltage drop over time under dynamic load conditions at a ramp rate of 5.0%/s

Current density (A/cm^2)	Voltage (V)								
	Initial	50 cycle	100 cycle	150 cycle	300 cycle	450 cycle	600 cycle	750 cycle	900 cycle
0.00	0.93	0.93	0.93	0.92	0.92	0.92	0.91	0.91	0.91
0.20	0.77	0.77	0.77	0.77	0.76	0.76	0.76	0.75	0.75
0.40	0.71	0.71	0.71	0.71	0.70	0.69	0.69	0.68	0.68
0.60	0.66	0.66	0.66	0.66	0.65	0.64	0.63	0.62	0.61
0.80	0.61	0.61	0.61	0.60	0.59	0.58	0.57	0.56	0.55
1.00	0.54	0.54	0.54	0.54	0.53	0.51	0.50	0.49	0.48
1.20	0.45	0.46	0.46	0.46	0.45	0.43	0.42	0.41	0.41

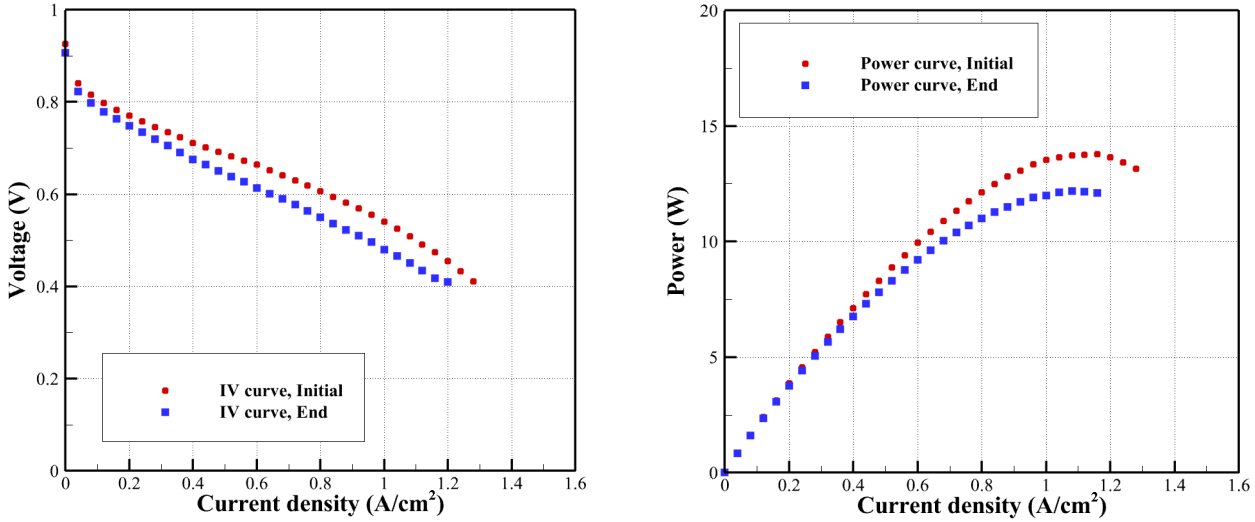

(a) (b)

Fig. 7 Comparison of (a) IV curves and (b) power curves at the initial and end stages (5.0% ramp rate)

range (Baragherabadi et al., 2022).

In general, the increased resistance of electrolyte membranes, the contact resistance between electrodes and current collectors, water management issues, and temperature management challenges are recognized as contributing factors to ohmic loss (Zhan et al., 2008; O'hayre et al., 2016). Given that there were no significant changes in temperature, humidity, ionization of humidifying water, electrodes, or current collectors, it can be inferred that the ohmic loss primarily resulted from the increased resistance of the electrolyte membranes. The observation that the voltage at the 1.00 A/cm² point was more significantly reduced compared to the static load condition indicates that the dynamic load condition is unfavorable with respect to ohmic loss. Therefore, it can be concluded that specific operational strategies must be developed to mitigate the increase in the resistance of electrolyte membranes when utilizing PEMFCs as the primary power source for ships. Since degradation due to dynamic loads is particularly pronounced in the relatively low current density range, implementing strategies for managing dynamic loads, such as using energy storage systems (e.g., auxiliary batteries) and operating PEMFCs under a constant load, is recommended in environments where ships operate at low speeds.

In the power curve presented in Fig. 6(b), the current density capable of producing the maximum power of the single cell is evident. A comparison of the power curves from the initial and end stages reveals a significant difference in maximum power before and after the long-term operation of the PEMFC. Specifically, the maximum power was observed at a current density of 1.28 A/cm² during the initial stage, whereas it decreased to 1.16 A/cm² in the end stage, within the measurement range limited to 0.40 V, which was implemented to protect the single cell. The initial power curve recorded a maximum value of 13.20 W at a current density of 1.20 A/cm². Notably, both the maximum current density and the output voltage at the same current density decreased following operation. Therefore, for the power curve depicted in Fig. 6(b), further investigation is required to analyze phenomena that deviate from the established trends, particularly through additional experiments focusing on current densities exceeding 1.20 A/cm².

Table 6 presents the voltage as a function of current density over time during the dynamic load experiment, in which a ramp rate of 5.0%/s was applied. Figs. 7(a) and 7(b) illustrate the current-voltage (IV) curve and power curve at the initial and end stages of the single cell utilized in the dynamic load experiment, respectively, under the same ramp rate of 5.0%/s. In Fig. 7(a), the voltage drop at the 1.00 A/cm² point was recorded at 0.061 V, three times higher than the

voltage drop of 0.022 V observed at the 0.20 A/cm² point. This finding indicates that ohmic loss was more predominant than activation loss during this experiment. The increased resistance of the electrolyte membranes is estimated to be a potential cause, consistent with the findings from the experiment conducted at a ramp rate of 2.5%/s, thereby reaffirming the necessity for separate operational strategies aimed at extending the lifespan of the electrolyte membranes. In the power curve shown in Fig. 7(b), a maximum power output of 13.77 W was achieved at a current density of 1.16 A/cm² during the initial stage, while a maximum power of 12.19 W was recorded at 1.08 A/cm² in the end stage. Although the characteristics of the output power varied in terms of maximum power and current density, they exhibited similar behavior to that observed in Fig. 6(b).

3.3 Degradation Rate

The three primary methods for calculating degradation rates, as presented in previous studies, are as follows: (1) a method that determines the degradation rate by dividing the difference between the initial and final voltage measurements in the time series by the total time (Cleghorn et al., 2006); (2) a method that calculates the voltage drop per hour using linear regression on the voltage-time series (Cheng et al., 2003); and (3) a method that derives the slope of the voltage drop through linear regression of the voltage time series classified by current density, based on the IV curve measured during the experiment (Chung et al., 2009).

In the current study, the degradation rate was calculated using the third method to eliminate external factors, such as disturbances caused

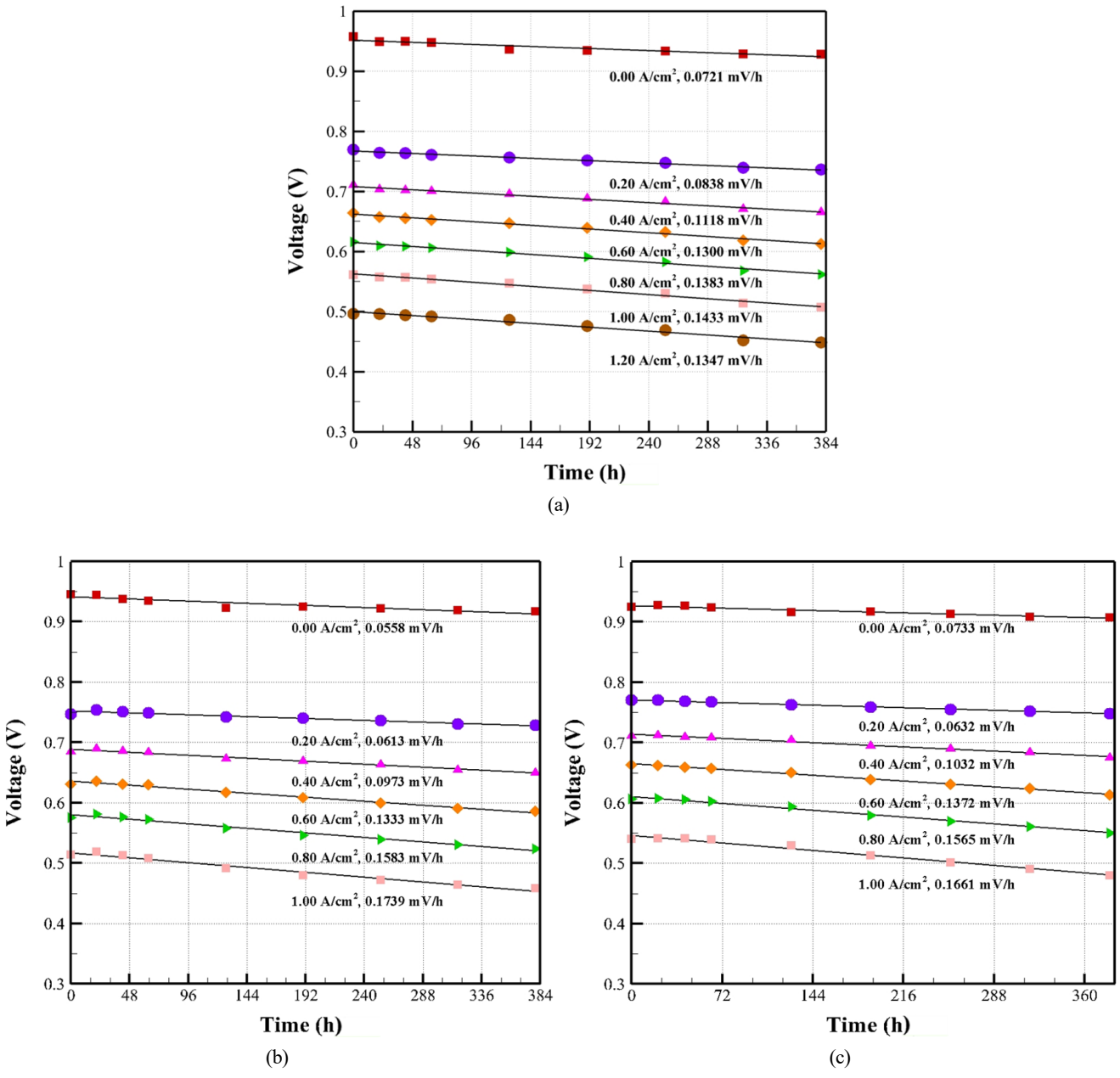

Fig. 8 Voltage time series at different current densities: (a) Static load condition (CC of 6.64 A); (b) Dynamic load condition with a ramp rate of 2.5%/s; (c) Dynamic load condition with a ramp rate of 5.0%/s

by the humidifier water supply, from the experimental results. To compare the extent of performance degradation in the single-cell experiment utilizing the MEA under different initial conditions, the voltage as a function of current density obtained from the IV curve was plotted over time (Fig. 8). In Fig. 8, the voltage decrease over time was classified for each current density, and trend lines were generated by performing linear regression on the voltage data at each current density. The linear regression analysis was conducted using the method of least squares in MATLAB (R2023a), and the derived degradation rates were indicated below the trend lines for each current density.

Fig. 9 shows the slopes of the trend lines calculated in Fig. 8 for each current density. The performance degradation rate corresponding to the increase in current load was compared through the degradation rates at different current densities. The average performance degradation rates were calculated to be 0.118 mV/h for a CC of 6.64 A, 0.120 mV/h for the load profile operation with a ramp rate of 2.5%/s, and 0.121 mV/h for the load profile operation with a ramp rate of 5.0%/s. The results from the 6.64 A CC experiment indicated that the degradation rate ranged from 0.094 to 0.100 mV/h during operation at a current density of 0.27 A/cm², which corresponds to 6.64 A. Additionally, the output voltage decreased most rapidly, with a degradation rate of 0.143 mV/h during operation at a current density of 1.00 A/cm^2. Under dynamic load conditions, at ramp rates of 2.5%/s and 5.0%/s, the output voltage decreased most rapidly at 0.167 mV/h at 1.04 A/cm^2 and 0.177 mV/h at 1.16 A/cm^2, respectively.

There was no significant difference in the degradation rate when the ramp rates were 2.5%/s and 5.0%/s. This observation appears to result from the oversupply of hydrogen and air at the stoichiometric ratio provided for cell protection. The excess gas seems to have mitigated the effects of starvation caused by the varying ramp rates of 2.5%/s and 5.0%/s. Consequently, further research is required at ramp rates exceeding 5.0%/s.

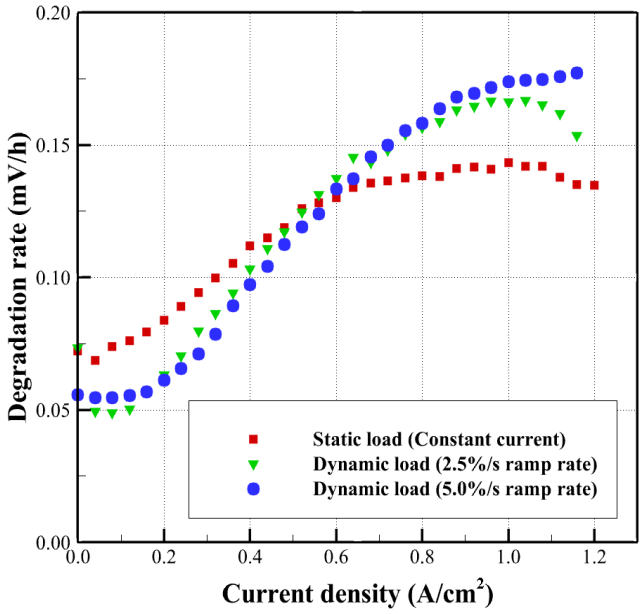

Fig. 9 Comparison of degradation rate at each current density

When comparing the degradation rates between the static and dynamic load conditions, the degradation rate at 1.00 A/cm^2 differed by 21% or more, indicating that the dynamic load of the ship can reduce the lifespan of the PEMFC by up to 21%. Furthermore, the degradation rate under dynamic load conditions was lower than that under static load conditions in the low current density range (0.20 A/cm²). This suggests that the lifespan of PEMFCs can be extended through operational strategies, such as low-speed operation, in environments characterized by high load fluctuations.

4. Conclusions

In this study, experiments were conducted using single cells to evaluate PEMFCs as a power source for ships. Analyzing the dynamic characteristics of PEMFC performance in relation to ship loads through these experiments led to the following conclusions.

Under static load conditions, performance degradation was predominant in the low current density range (0.40 A/cm² or less), and the difference in degradation rates compared to dynamic load conditions increased as the current density increased, attributed to the dominance of ohmic losses in dynamic load conditions, as confirmed by the comparative analysis of the degradation rates quantifying performance degradation. The degradation rate differed by as much as three-fold, indicating that distinct operational strategies are necessary to extend the lifespan of PEMFCs when utilized as the primary power source for ships.

Under dynamic load conditions, varying ramp rates of 2.5%/s and 5.0%/s did not affect performance characteristics. This lack of variation appears to stem from the ramp rate difference being insufficient to induce starvation in the single cell, as well as the oversupply of hydrogen and air, which served to mitigate potential damage to the cell, thereby offsetting the effects of the ramp rate. Future research should focus on optimizing the gas supply to enhance PEMFC performance in marine applications.

Ship operating conditions were represented by simplifying the ship loads to include loading, unloading, maneuvering, and seagoing activities. A comparison with static load conditions was conducted using this simplified load profile, revealing that the degradation rate differed by up to 21%. While the load profile employed in this study included loading, unloading, maneuvering, and seagoing, it did not account for load fluctuations caused by external factors. Therefore, future research should investigate the performance characteristics in relation to dynamic loads under conditions more representative of actual ship operations, incorporating external factors.

Conflict of Interest

No potential conflict of interest relevant to this article was reported.

Funding

This research was supported by Regional Innovation Strategy (RIS) through the National Research Foundation of Korea (NRF) funded by the Ministry of Education (MOE) (2023RIS-007) and 2-Year Research Grant of Pusan National University.

References

Bagherabadi, K. M., Skjong, S., Bruinsma, J., & Pedersen, E. (2022). System-level modeling of marine power plant with PEMFC system and battery. *International Journal of Naval Architecture and Ocean Engineering*, *14*, 100487. https://doi.org/10.1016/j.ijnaoe.2022.100487

Cheng, X., Chen, L., Peng, C., Chen, Z., Zhang, Y., & Fan, Q. (2003). Catalyst microstructure examination of PEMFC membrane electrode assemblies vs. time. *Journal of the Electrochemical Society, 151*(1), A48. https://doi.org/10.1149/1.1625944

Chu, T., Wang, Q., Xie, M., Wang, B., Yang, D., Li, B., .Ming, P., & Zhang, C. (2022). Investigation of the reversible performance degradation mechanism of the PEMFC stack during long-term durability test. *Energy, 258*, 124747. https://doi.org/10.1016/j.energy.2022.124747

Chung,C.G.,Kim,L.,Sung,Y.W.,Lee,J.,&Chung,J.S.(2009).Degradation mechanism of electrocatalyst during long-term operation of PEMFC . *International Journal of Hydrogen Energy, 34*(21), 8974–8981. https://doi.org/10.1016/j.ijhydene.2009.08.094

Cleghorn, S. J. C., Mayfield, D. K., Moore, D. A., Moore, J. C., Rusch, G., Sherman, T. W., Sherman, T. W., & Beuscher, U. (2006). A polymer electrolyte fuel cell life test: 3 years of continuous operation. *Journal of Power Sources, 158*(1), 446–454. https://doi.org/10.1016/j.jpowsour.2005.09.062

Elkafas, A. G., Rivarolo, M., Gadducci, E., Magistri, L., & Massardo, A. F. (2022). Fuel cell systems for maritime: a review of research development, commercial products, applications, and perspectives. *Processes, 11*(1), 97. https://doi.org/10.3390/pr11010097

Gadducci, E., Lamberti, T., Rivarolo, M., & Magistri, L. (2022). Experimental campaign and assessment of a complete 240-kW Proton Exchange Membrane Fuel Cell power system for maritime applications. *International Journal of Hydrogen Energy, 47*(53), 22545–22558. https://doi.org/10.1016/j.ijhydene.2022.05.061

Hassani, M., Rahgoshay, M., Rahimi-Esbo, M., & Dadashi Firouzjaei, K. (2020). Experimental study of oxidant effect on lifetime of PEM fuel cell. *Hydrogen, Fuel Cell & Energy Storage, 7*(1), 33–43. https://doi.org/10.22104/ijhfc.2020.4068.1202

Hou, K. H., Lin, C. H., Ger, M. D., Shiah, S. W., & Chou, H. M. (2012). Analysis of the characterization of water produced from proton exchange membrane fuel cell (PEMFC) under different operating thermal conditions. *International journal of hydrogen energy, 37*(4), 3890–3896. https://doi.org/10.1016/j.ijhydene.2011.05.129

International Electrotechnical Commission (IEC). (2017). *IEC Technical Specification 62282-7-1 Fuel cell technologies - Part 7-1: Test methods - Single cell performance tests for polymer electrolyte fuel cells (PEFC)*. https://webstore.iec.ch/publication/31478

Lee, G. N., Kim, J. M., Jung, K. H., Park, H., Jang, H. S., Lee, C. S., & Lee, J. W. (2022). Environmental life-cycle assessment of eco-friendly alternative ship fuels (MGO, LNG, and hydrogen) for 170 GT nearshore ferry. *Journal of Marine Science and Engineering, 10*(6), 755. https://doi.org/10.3390/jmse10060755

Lee, G. Y., Jung, M. K., Ryoo, S. N., Park, M. S., Ha, S. C., & Kim, S. (2010). Development of cost innovative BPs for a PEMFC stack for a 1 kW-class residential power generator (RPG) system. *International journal of hydrogen energy, 35*(23), 13131–13136. https://doi.org/10.1016/j.ijhydene.2010.04.081

Meng, K., Zhou, H., Chen, B., & Tu, Z. (2021). Dynamic current cycles effect on the degradation characteristic of a H_2/O_2 proton exchange membrane fuel cell. *Energy, 224*, 120168. https://doi.org/10.1016/j.energy.2021.120168

Oh, S., Lee, M., Lee, H., Kim, W., Park, J. W., & Park, K. (2018). Performance comparison between stationary PEMFC MEA and automobile MEA under pure hydrogen supply condition. *Korean Chemical Engineering Research, 56*(4), 469–473. https://doi.org/10.9713/kcer.2018.56.4.469

O'hayre, R., Cha, S. W., Colella, W., & Prinz, F. B. (2016). *Fuel cell fundamentals*. John Wiley & Sons. https://doi.org/0.1002/9781119191766

Paperzh, K., Alekseenko, A., Pankov, I., & Guterman, V. (2024). Accelerated stress tests for Pt/C electrocatalysts: An approach to understanding the degradation mechanisms. *Journal of Electroanalytical Chemistry, 952*, 117972. https://doi.org/10.1016/j.jelechem.2023.117972

Park, S. K., & Choe, S. Y. (2008). Dynamic modeling and analysis of a 20-cell PEM fuel cell stack considering temperature and two-phase effects. *Journal of Power Sources, 179*(2), 660–672. https://doi.org/10.1016/j.jpowsour.2008.01.029

Saponaro, G., Stefanizzi, M., Torresi, M., & Camporeale, S. M. (2024). Analysis of the degradation of a Proton Exchange Membrane Fuel Cell for propulsion of a coastal vessel. *International Journal of Hydrogen Energy, 61*, 803–819. https://doi.org/10.1016/j.ijhydene.2024.02.349

Tian, P. (2020). *Performance prediction of PEM fuel cell using artificial neural network machine learning*. University of California, Irvine.

Wasterlain, S., Candusso, D., Hissel, D., Harel, F., Bergman, P., Menard, P., & Anwar, M. (2010). Study of temperature, air dew point temperature and reactant flow effects on PEMFC performances using electrochemical spectroscopy and voltammetry techniques. *Journal of Power Sources, 195*(4), 984–984. https://doi.org/10.1016/j.jpowsour.2009.08.084

Zhan, Y., Zhu, J., Guo, Y., & Wang, H. (2008, October). Performance analysis and improvement of a proton exchange membrane fuel cell using comprehensive intelligent control. In *2008*

international conference on electrical machines and systems (pp. 23782383). IEEE.

Zuo, J., Lv, H., Zhou, D., Xue, Q., Jin, L., Zhou, W., Yang, D., & Zhang, C. (2021). Deep learning based prognostic framework towards proton exchange membrane fuel cell for automotive application. *Applied Energy, 281*, 115937. https://doi.org/10.1016/j.apenergy.2020.115937

Author ORCIDs

Author name	ORCID
Kim, Jae hong	0000-0003-0384-878X
Lee, Seon hyoeng	0009-0009-2631-7763
Kwon, Jae heon	0009-0001-9868-4951
Kwon, Ryu bin	0009-0005-8960-9836
Jung, Kwang hyo	0000-0002-8229-6655
Son, Moonho	0009-0001-0831-0738
Park, Hyun	0000-0001-5510-3670